


Electronic structure of chromium trihalides beyond density functional theorySwagata Acharya^{1,*}, Dimitar Pashov,² Brian Cunningham³, Alexander N. Rudenko¹, Malte Rösner¹, Myrta Grüning,⁴ Mark van Schilfgaarde,^{2,5} and Mikhail I. Katsnelson¹¹*Institute for Molecules and Materials, Radboud University, NL-6525 AJ Nijmegen, The Netherlands*²*King's College London, Theory and Simulation of Condensed Matter, The Strand, WC2R 2LS London, United Kingdom*³*Centre for Theoretical Atomic, Molecular and Optical Physics,**Queen's University Belfast, Belfast BT71NN, Northern Ireland, United Kingdom*⁴*Atomistic Simulation Centre, Queen's University Belfast, Belfast BT71NN, Northern Ireland, United Kingdom*⁵*National Renewable Energy Laboratory, Golden, Colorado 80401, USA* (Received 16 June 2021; revised 28 August 2021; accepted 22 September 2021; published 5 October 2021)

We explore the electronic band structure of freestanding monolayers of chromium trihalides CrX_3 , $X = \text{Cl}, \text{Br}, \text{I}$, within an advanced *ab initio* theoretical approach based on the use of Green's function functionals. We compare the local density approximation with the quasiparticle self-consistent GW (QSGW) approximation and its self-consistent extension (QSG \widehat{W}) by solving the particle-hole ladder Bethe-Salpeter equations to improve the effective interaction W . We show that, at all levels of theory, the valence band consistently changes shape in the sequence $\text{Cl} \rightarrow \text{Br} \rightarrow \text{I}$, and the valence band maximum shifts from the M point to the Γ point. By analyzing the dynamic and momentum-dependent self-energy, we show that QSG \widehat{W} adds to the localization of the systems in comparison with QSGW, thereby leading to a narrower band and reduced amount of halogens in the valence band manifold. Further analysis shows that $X = \text{Cl}$ is most strongly correlated, and $X = \text{I}$ is least correlated (most bandlike) as the hybridization between Cr d and X p enhances in the direction $\text{Cl} \rightarrow \text{Br} \rightarrow \text{I}$. For CrBr_3 and CrI_3 , we observe remarkable differences between the QSGW and QSG \widehat{W} valence band structures, while their eigenfunctions are very similar. We show that weak perturbations, like moderate strain, weak changes to the d - p hybridization, and adding small U , can flip the valence band structures between these two solutions in these materials.

DOI: [10.1103/PhysRevB.104.155109](https://doi.org/10.1103/PhysRevB.104.155109)**I. INTRODUCTION**

With the discovery of ferromagnetic order in CrI_3 , the family of chromium trihalides CrX_3 , $X = \text{Cl}, \text{Br}, \text{I}$, has emerged as a class of magnetic two-dimensional (2D) crystals. Ferromagnetism (FM) in a monolayer (ML) CrI_3 was reported [1,2], which was followed by observation of FM in CrBr_3 [3,4], CrCl_3 [5], and many other compounds [6–10]. FM is intrinsic to these systems, which distinguishes them from traditional 2D sp -electron magnets, where magnetism is induced by proximity to a FM substrate. Long-range order is typically suppressed in 2D magnets [11], but it can be stabilized by magnetocrystalline anisotropy, which opens an energy gap in the magnon spectra and therefore protects the FM in 2D [12,13]. Due to their layered structure and their weak interlayer van der Waals interactions, these systems are loosely coupled to their substrates, which provides greater flexibility in functionalizing them and controlling their properties, e.g., by varying the layer number or by applying a gate voltage. This offers possibilities to make spintronic devices with high accuracy and efficiency [2,14–22].

CrX_3 is a 2D FM insulator with FM originating from the Cr-X-Cr superexchange interaction [13,23–25]. Six Cr^{3+} ions

form a honeycomb structure with D_{3d} point group symmetry, and each Cr is surrounded by six X in an octahedral geometry (see Fig. 1). The edge-sharing geometry leads to first neighbor Cr atoms sharing a pair of ligands. This enables pathways for Cr-X-Cr superexchange. In this crystal field geometry, the Cr d splits into a t_{2g} triplet and an e_g doublet. Cr^{3+} has a valence of three electrons, which fill the t_{2g} majority-spin band according to Hund's first rule, leaving all other d bands empty. The ionic model leads to the magnetic moment on each Cr^{3+} ion of $\sim 3\mu_B$, which is confirmed by *ab initio* calculations.

All three CrX_3 compounds have FM order down to the ML with Curie temperatures $T_{\text{I}} = 45$ K [1], $T_{\text{Br}} = 34$ K [3], and $T_{\text{Cl}} = 17$ K [5], and the magnetization easy axis is normal to the plane for CrI_3 and CrBr_3 , while it is in plane for CrCl_3 .

Recent density functional theory [local density approximation (LDA)] calculations [26–28] confirm the qualitative understandings derived from the ionic model. However, at quantitative level, details start to differ from the fully ionic picture; one important such factor is the degree of hybridization of the t_{2g} levels with the p bands of the ligands. This degree of hybridization depends on the ligand, its atomic weight, and the number of core levels, which turns out to be a crucially important factor in determining the detailed electronic band structure. This is the main focus of this paper, which we carefully analyze on different levels of theory beyond conventional density functional theory. Our

*swagata.acharya@ru.nl

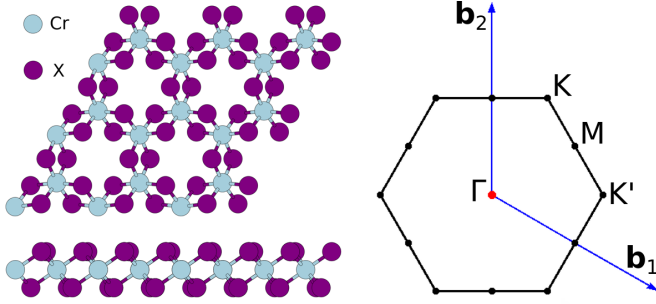


FIG. 1. Left: Ball-and-stick model of the crystal structure of monolayer chromium trihalides CrX_3 ($X = \text{Cl}, \text{Br}, \text{I}$). Right: Brillouin zone of the corresponding hexagonal lattice with the high-symmetry points indicated. \mathbf{b}_1 and \mathbf{b}_2 denote reciprocal lattice vectors.

quasiparticle self-consistent GW (QSGW) and Bethe-Salpeter equation (BSE; QSGW) implementations are independent of the starting point and, hence, allow us to study the roles of self-consistent charge densities and self-energies in determining the key features of the electronic structures at different levels of the theory. Within our fully self-consistent diagrammatic many-body perturbative first-principles approach, the electronic eigenfunctions keep changing with additional diagrams and across the three different materials, depending on the nature of the ligand.

II. MOLECULAR PICTURE

Within the LDA, we find the spin-polarized band gaps of the three systems to be 1.51, 1.30, and 1.20 eV for $X = \text{Cl}, \text{Br}, \text{I}$, respectively, in line with prior work [26]. The qualitative trend is easily understood in terms of the splitting between $\text{Cr } d$ and $X p$ atomic levels. In the simplest two-level tight-binding description, the conduction and valence levels are given by $(\varepsilon_d + \varepsilon_p)/2 \pm \sqrt{[(\varepsilon_d - \varepsilon_p)/2]^2 + v^2}$, where ε_d and ε_p are, respectively, the $\text{Cr } t_{2g} d$ and $X p$ atomic levels and v the hybridization matrix element. This results in a gap $E_g = \varepsilon_d - \varepsilon_p + 2v^2/(\varepsilon_d - \varepsilon_p)$ to the lowest order in $v/(\varepsilon_d - \varepsilon_p)$. Among all three halides, iodine has the most core levels, resulting in its p levels having the most nodes which thus sense the attractive nucleus most weakly. It has the shallowest ε_p of the three halogens, while Cl has the deepest. Thus, the qualitative trend in the band gap is simply understood as following from the halide ε_p energies relative to the $\text{Cr } \varepsilon_d$. As

TABLE I. One-particle electronic band gap at different levels of theory (with spin-orbit coupling) for both bulk and ML variants. The gap increases from LDA to QSGW level. When ladder diagrams are added, two-particle interactions via a BSE, $W \rightarrow \widehat{W}$, and screening is increased. This reduces the QSGW band gap. Right columns show fraction of spectral weight that the halogen contributes to the total DOS within an energy window of occupied states ($-0.6, 0$) eV, relative to the valence band maximum. Bulk QSGW band gaps are 20–25% smaller than their ML variants.

Theory	ML band gap (eV)			ML spectral weight			Bulk band gap (eV)		
	CrCl ₃	CrBr ₃	CrI ₃	CrCl ₃	CrBr ₃	CrI ₃	CrCl ₃	CrBr ₃	CrI ₃
LDA	1.51	1.30	1.06	21%	26%	42%	1.38	1.2	0.91
QSGW	6.87	5.73	3.25	40%	63%	81%	5.4	4.38	3.0
QSGW	5.55	4.65	2.9	24%	31%	64%	4.4	3.5	2.5

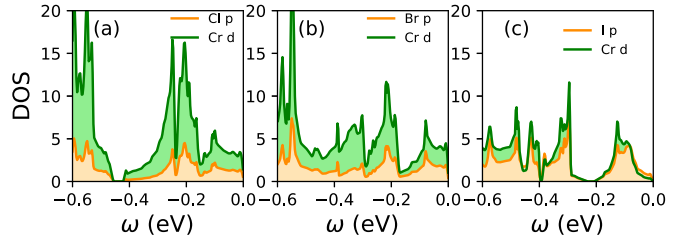


FIG. 2. Partial density of states within the local density approximation (LDA), projected onto the $\text{Cr } d$ and $X p$ states for (a) $X = \text{Cl}$, (b) Br , and (c) I

a slight elaboration on this picture that includes magnetism, we can distinguish between the majority (t_{2g}^\uparrow) and minority (t_{2g}^\downarrow) $\text{Cr } d$ levels. For the band gap, the picture just sketched corresponds to the $(\varepsilon_d^\downarrow - \varepsilon_p)$ bond. A similar picture applies to the $\varepsilon_d^\uparrow - \varepsilon_p$ bond, but in this channel, both bond and antibond are occupied, and moreover, $\varepsilon_d^\uparrow - \varepsilon_p$ need not be large in comparison to v . Indeed, the $\text{Cr } t_{2g}^\uparrow$ and $X p$ levels may overlap.

III. ENERGY BAND PICTURE

The molecular picture qualitatively explains the trends in the band gap and the admixture of $X p$ in the highest valence states in the sequence $\text{Cl} \rightarrow \text{Br} \rightarrow \text{I}$. However, in the 2D crystal, the molecular levels broaden into bands which can alter the trends in both the band gap and the merging of $X p$ with $\text{Cr } t_{2g}^\uparrow$ in the valence bands. The corresponding orbital resolved density of states (DOS) are shown in Fig. 2. The $X p$ level becomes more shallow, and the highest lying valence band acquires increasing anion character, as can be seen in both Table I and Fig. 2. Spin-orbit coupling only slightly modifies the electronic structure for CrCl_3 and CrBr_3 , while for CrI_3 , the band gap reduces by 150 meV to 1.06 eV in the LDA.

However, as is typical of the LDA, the band gaps are underestimated, and for CrX_3 , the underestimation is severe. Accordingly, we study the electronic structure at three different levels of theory: the LDA, the QSGW [29,30], and an extension of QSGW where the random phase approximation (RPA) to the polarizability is extended by adding ladder diagrams (QSGW) [31,32]. The electronic dispersions and corresponding DOS are shown in Figs. 3–5 for each level of theory and each material. In contrast to typical sp semiconductors, not only the band gaps but also the valence

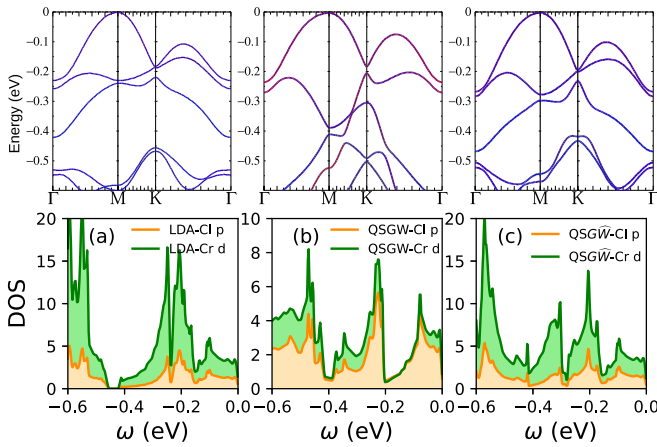


FIG. 3. CrCl_3 : From left to right: local density approximation (LDA), quasiparticle self-consistent GW (QSGW), and its self-consistent extension (QSGW) valence band structures (with spin-orbit coupling) are shown, respectively. The colors correspond to Cl $p_x + p_y$ (red), Cl p_z (green), and Cr d (blue). In the bottom panels are shown the density of states projected onto the Cr d and Cl p states at different levels of the theory.

band dispersions significantly change as the level of theory increases.

QSGW dramatically enhances the gaps relative to the LDA, as is standard in polar compounds [29]. Nevertheless, within the RPA, it has long been known that W is universally too large [33,34], and this is reflected in an underestimate of the static dielectric constant ϵ_∞ . Empirically, ϵ_∞ seems to be underestimated in QSGW by a nearly universal factor of 0.8 for a wide range of insulators [35,36]. Roughly speaking, at

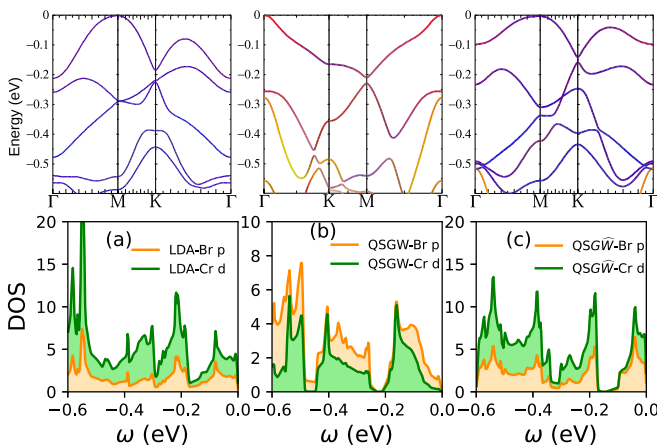


FIG. 4. CrBr_3 : From left to right: local density approximation (LDA), quasiparticle self-consistent GW (QSGW), and its self-consistent extension (QSGW) valence band structures (with spin-orbit coupling) are shown, respectively. The colors correspond to Br $p_x + p_y$ (red), Br p_z (green), and Cr d (blue). In the bottom panels are shown the density of states projected onto the Cr d and Br p states at different levels of the theory. The structure of the topmost valence band is similar within LDA and QSGW but is different in QSGW. The QSGW topmost valence band is much narrower than both QSGW and LDA and is split from the rest of the valence band manifold.

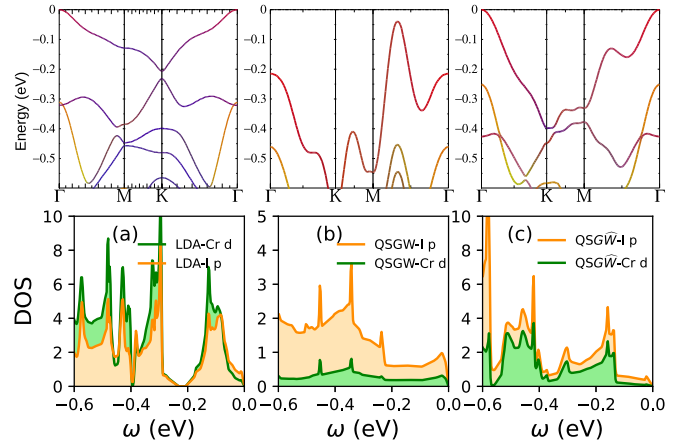


FIG. 5. CrI_3 : From left to right: local density approximation (LDA), quasiparticle self-consistent GW (QSGW), and its self-consistent extension (QSGW) valence band structures (with spin-orbit coupling) are shown, respectively. The colors correspond to I $p_x + p_y$ (red), I p_z (green), and Cr d (blue). In the bottom panels are shown the density of states projected onto the Cr d and I p states at different levels of the theory. Note that, in the QSGW case, the valence band maximum is at a low-symmetry point not on the lines of the figure.

low energy, W is universally too large by a factor of $\frac{1}{0.8}$ [37], and as a result, QSGW band gaps are slightly overestimated [29]. This can be corrected by extending the RPA to introduce an electron-hole attraction in virtual excitations. These extra (ladder) diagrams are solved by a BSE, and they significantly improve on the optics, largely eliminating the discrepancy in ϵ_∞ [31]. When ladders are also added to improve W in the GW cycle ($W \rightarrow \tilde{W}$), it significantly improves the one-particle gap as well, as will be discussed elsewhere [32]. This scenario is played out in CrX_3 compounds: QSGW band gaps are slightly larger than QSGW band gaps, as seen in Table I. We note that the QSGW band gaps for the bulk variants come out $\sim 20\text{--}25\%$ smaller (see Table I) than their ML counterparts due to enhanced screening in the bulk; nevertheless, their involved band structural details remain similar.

Remarkably, the structure of the valence band is very sensitive to the level of theory used, which applies to both, the band energies and wave functions. Just for CrCl_3 the valence band maximum is independent of the theory and is consistently pinned to the M point (Fig. 3). In the sequence $\text{Cl} \rightarrow \text{Br} \rightarrow \text{I}$, there is an overall tendency for the valence band maximum to shift from the M point to the Γ point. In the LDA, this transition occurs after Br and I, while in QSGW, the valence band at Γ is above M already for Br. QSGW shows the same tendency as QSGW, but the change is less pronounced, and the transition takes place between Br and I. This is a reflection of the softening effects of the ladder diagrams on W .

A. Structure of valence bands

To understand this curious renormalization of valence bands between different levels of the theory, we perform a series of parametric studies. The key point is the dramatic renormalization in the valence band structure between QSGW

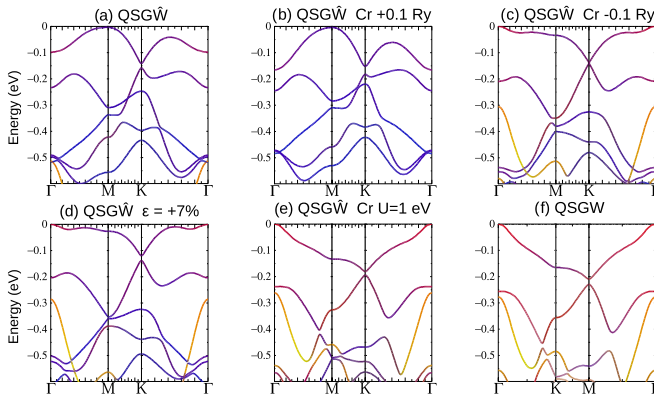


FIG. 6. CrBr_3 : The quasiparticle self-consistent GW extension ($\text{QSG}\widehat{W}$) valence band structures (with spin-orbit coupling) are shown under different perturbations. Weak perturbations can modify the Cr d and Br p hybridization and qualitatively modify the valence band structure. (a) and (f) The unperturbed $\text{QSG}\widehat{W}$ and quasiparticle self-consistent GW (QSGW) valence band structures. (b) Cr + 0.1 Ry is the $\text{QSG}\widehat{W}$ solution after shifting the Cr d band center up by 0.1 Ry. (c) Cr - 0.1 Ry is the $\text{QSG}\widehat{W}$ solution after shifting the Cr d band center down by 0.1 Ry. (d) $\epsilon = 7\%$ is the $\text{QSG}\widehat{W}$ solution with 7% volume conserving strain along (001). (e) $\text{QSG}\widehat{W} + U$ solution with $U = 1$ eV on the Cr d . The colors correspond to $I p_x + p_y$ (red), $I p_z$ (green), and Cr d (blue).

and $\text{QSG}\widehat{W}$ for CrBr_3 and CrI_3 . For CrBr_3 , the valence band maximum is at M in $\text{QSG}\widehat{W}$ and at Γ in QSGW . Also, the Br p content is significantly enhanced in the valence bands in QSGW , as can be seen in Fig. 4(b), compared with $\text{QSG}\widehat{W}$ [see Fig. 4(c) and Table I]. We perform $\text{QSG}\widehat{W}$ calculations by (a) applying volume conserving strains (ϵ) along (001), (b) shifting the center of mass of Cr d up by 0.1 Ry (Cr + 0.1 Ry), (c) shifting the center of mass of Cr d down by 0.1 Ry (Cr - 0.1 Ry), (d) applying $U = 1$ eV on the Cr d (Cr $U = 1$ eV). We see that the valence band structure does not have any dramatic qualitative change [see Fig. 6(b)] in the case of Cr + 0.1 Ry. By shifting the Cr d band center up by 0.1 Ry, we effectively reduce the hybridization between Cr d and $X p$ moderately. This can be observed in the color projection for the topmost valence band as it becomes more blue (Cr d orbitals) compared with Fig. 6(a), which has significant red component (Br p). However, the reverse Cr - 0.1 Ry hybridizes more the Cr d and Br p , and the valence band [see Fig. 6(c)] starts looking more similar to QSGW results [see Fig. 6(f)]. A similar situation emerges when tensile strain $\epsilon = 7\%$ is applied [see Fig. 6(d)]. However, we derive the most understanding when $U = 1$ eV is applied on the Cr d . Applying U shifts the Cr majority spin down and the minority spin up. The gap widens, becomes 5.10 eV compared with 4.65 eV without U , but at the same time increases hybridization with the Br p . The valence band structure [see Fig. 6(e)] looks like the one from QSGW . In short, the self-consistent eigenfunctions from $\text{QSG}\widehat{W} + U$ are identical with QSGW . This also establishes the fact that, albeit their apparent dissimilarities, the $\text{QSG}\widehat{W}$ and QSGW solutions are quite similar, and it is possible to flip between the two by applying weak perturbations. This is intriguing, as it implies that it would also be possible

to dramatically alter the valence band structures of CrX_3 in real-world experiments with weak perturbations. We observe that the situation is similar in bulk as well, where for CrBr_3 and CrI_3 , the valence band structure is qualitatively different between QSGW and $\text{QSG}\widehat{W}$. Altogether, they suggest that the source of this observation lies in the details of the W and not in the dimensionality of the materials. The fact that the $\text{QSG}\widehat{W}$ and QSGW are identical for $X = \text{Cl}$ and most different in $X = \text{I}$, can now naturally be understood. In $X = \text{I}$, the $I p$ states are the shallowest compared with the Cr d states, and hence, to change the valence band manifold by tweaking Cr d and $I p$ hybridization is easy in CrI_3 , while it is most difficult in CrCl_3 .

Recent works implementing single-shot GW , with approximations different from QSGW , also found the valence band maximum in CrI_3 at Γ [26,38], which also seems to be confirmed by a recent angle-resolved photoemission spectroscopy study [39]. Two recent theoretical works report one-particle band gaps of 2.23 and 1.57 eV, respectively, from QSGW [40] and $\text{QSGW} + \text{BSE}$ [41]. Lee *et al.* [40] used a manually scaled $\text{QSGW}\Sigma$ to produce the gap of 2.23 eV. Note that their estimate for band gap is very similar to our bulk estimate of 2.5 eV and smaller than our ML estimate of 2.9 eV. Presumably, their valence band structure from QSGW is different from ours because of the manual scaling of Σ . For CrI_3 , Kutepov [41] included vertex corrections both in W and Σ to produce the gap of 1.57 eV. This is a significant difference from our $\text{QSG}\widehat{W}$ implementation, and we can expect the results to be different. Also, as we discussed above, in cases with Cr - 0.1 Ry and $\epsilon = 7\%$, the electronic gap reduces in both cases. One can expect this to be qualitatively the direction where the band gap approaches as the vertex is explicitly incorporated in Σ , in the spirit of the smaller band gap that Kutepov found from his implementation. However, it is not clear from these works [40,41] whether the vacuum corrections were incorporated or not. Vacuum corrections in our method lead to enhancement in band gap by ~ 0.3 – 0.4 eV. Hence, a rigorous comparison of the absolute value of the band gap against our findings is difficult. In another work, Wu *et al.* [42] achieved one-particle band gap of 3.8 eV in G_0W_0 in CrBr_3 . They used a local spin density approximation (LSDA) + U starting mean-field potential with choices of $U = 1.5$ eV and $J = 0.5$ eV for their one-shot G_0W_0 . However, G_0W_0 only updates the LSDA + U eigenvalues but does not change the eigenfunctions. Also, our implementation being fully self-consistent and starting-point independent, we do not have any free parameters like U and/or J . In a separate work, Molina-Sanchez *et al.* [26] employed G_0W_0 with LSDA + U starting parameters that are completely consistent with the work by Wu *et al.* [42]. However, Molina-Sanchez *et al.* [26] achieved a band gap of 4.45 eV for CrBr_3 . However, G_0W_0 is known to produce smaller band gaps than QSGW . Furthermore, QSGW systematically produces larger band gaps since W gets underscreened via self-consistency, which is corrected as ladder diagrams are incorporated in W . This we can see, as our estimate for the $\text{QSG}\widehat{W}$ band gap of 4.65 eV is closer to the G_0W_0 estimate of 4.45 eV by Molina *et al.* [26]. Note that, in bulk variants, we achieve band gaps which are $\sim 20\%$ smaller in all cases than their ML variants. Again, in both the works from Wu *et al.* [42] and Molina *et al.* [26], we did not

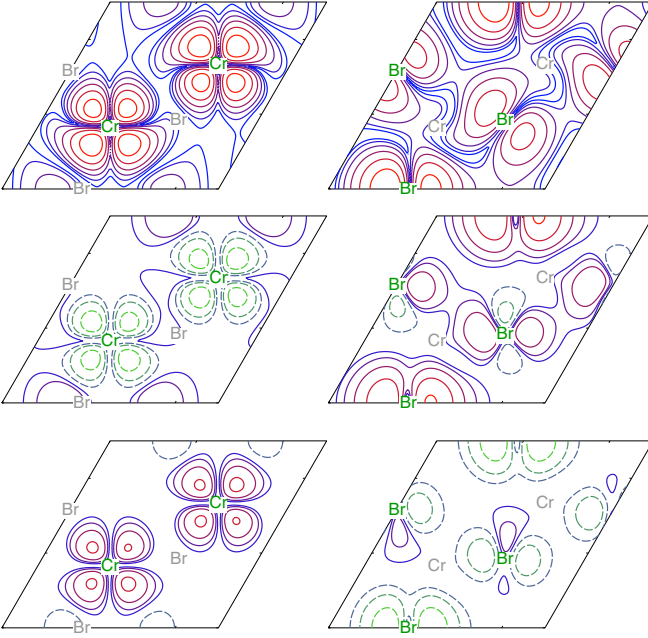


FIG. 7. CrBr₃: Square of wave function ψ , in real space, of the highest valence band state at the M point. All the left panels pass through a Cr plane, and right panels pass through a Br plane. Cr and Br site positions are labeled in green in the plane where they reside and gray when they lie in a different plane. Top panels display constant-amplitude contours for local density approximation (LDA) eigenfunctions. Contours are taken in half-decade increments in $|\psi|^2$, with a factor of 300 between highest contour (red) and lowest (blue). In the Cr plane, the atomic d_{xy} character centered at Cr nuclei stand in sharp relief; in the Br plane, the Br atomic p character is evident. Middle panels show the change in $|\psi|^2$ passing from LDA to quasiparticle self-consistent GW (QSGW) eigenfunctions; bottom panels show the corresponding change passing from QSGW to its self-consistent extension (QSGW \hat{W}) eigenfunctions. In the bottom four panels, blue \rightarrow red has a similar meaning as in the top panels (increasing positive $\delta|\psi|^2$), while contours of negative $\delta|\psi|^2$ are depicted by increasing strength in the change blue \rightarrow green. Note that the color patterns in the middle and bottom panels are mirror images. As a consequence of the softening in W in the change $W \rightarrow \hat{W}$, the shift in density LDA \rightarrow QSGW is partially reversed by the addition of ladder diagrams.

find any comments on the vacuum corrections. In CrBr₃, in the absence of the vacuum corrections, we achieved a gap of 4.26 eV from our QSGW \hat{W} implementation, which is much closer to the estimates from the works that used G_0W_0 .

To further understand these remarkable changes in the valence band structures, we analyzed the electronic eigenfunctions from different levels of the theory. Even though the QSGW \hat{W} band structure more closely resembles LDA than QSGW, the eigenfunctions do not. This can be seen by inspecting the square of the wave function $|\psi|^2$ corresponding to the highest-lying state at the M point (Fig. 7). The density is plotted in real space, and the abscissa and ordinate are defined by the inverse transpose of the 2×2 matrix composed of \mathbf{b}_1 and \mathbf{b}_2 in Fig. 1. Throughout this paper, x and y are defined by aligning \mathbf{b}_2 parallel to y . In this notation, the M point is on the \mathbf{b}_2 line or the y axis. Contour plots in two planes are

TABLE II. Effective masses m^*/m_0 at the M point (as shown in Fig. 1) for CrCl₃ and CrBr₃, and at the Γ point for CrI₃, for three levels of approximation. These k points correspond to the valence band maximum except for CrBr₃ in the QSGW approximation (see Fig. 5). m_x and m_y correspond to orientations perpendicular and parallel to the Γ - M line, respectively. ∞ is a shorthand for an effective mass larger than $10m_0$.

Theory	CrCl ₃		CrBr ₃		CrI ₃	
	m_x	m_y	m_x	m_y	m_x	m_y
LDA	1.9	3.6	2.0	5.2	1.2	1.2
QSGW	2.3	5.5	∞	-1.3	1.4	1.4
QSGW \hat{W}	2.1	4.2	3.2	∞	0.57	0.57

shown passing through Cr and Br, respectively. At the LDA level (top panels), the wave function resembles an atomic d_{xy} state centered at each Cr nucleus. In the Br plane, some Br p character is evident, and the bond is partially directed along x . The middle panels depict the change in $|\psi|^2$ when passing from LDA to QSGW. Two effects are prominent: First, there is a transfer of spectral weight from Cr to Br (mostly green contours on Cr, red on Br), as also noted in Table I. Second, the bonding becomes more directional, forming one-dimensional chains along x . This reflects an enhancement of the Cr-Cr coupling mediated through the Br. It is especially apparent in the Br plane, but it is also reflected in the asymmetry between the x and y directions in the Cr plane. The bottom two panels show the change in $|\psi|^2$ when passing from QSGW to QSGW \hat{W} . Here, QSGW \hat{W} seems to undo some effect of QSGW, although the changes remain moderate. This suggests that the QSGW and QSGW \hat{W} eigenfunctions are not significantly different.

The directionality in the wave function is also reflected in strong anisotropy in the valence band mass at the point M , particularly in CrBr₃ (see Table II). By symmetry, there is no anisotropy at the Γ point, but at M , it becomes quite pronounced at the highest level of theory.

Finally, we analyze the dynamic and momentum-dependent self-energies $\Sigma(k, \omega)$ from QSGW and QSGW \hat{W} to further understand the changes in the valence band structure at different levels of theory. We observe that the Σ of the topmost valence band has very weak dependence on momentum. The momentum dependence is even weaker in the down-spin channel that is unoccupied. For the up-spin channel, the momentum dispersion is very similar, both in QSGW and QSGW \hat{W} . We extract the quasiparticle renormalization (Z_k) factors from $\Sigma(k, \omega)$ at the quasiparticle energies for the topmost valence band. We observe that Z_k reduces by $\sim 20\%$ (see Fig. 8) within QSGW \hat{W} in comparison with QSGW. This suggests that the quasiparticles become further localized at the QSGW \hat{W} level, in comparison with the QSGW. This goes along with charge density that is weakly put back on the atoms at the QSGW \hat{W} level.

IV. CONCLUSIONS

We analyzed in detail the electronic band structure of CrX₃ within different levels of an *ab initio* theory. The results were interpreted in terms of a simplified tight-binding model to elucidate the trends in Cl \rightarrow Br \rightarrow I, particularly the band gap

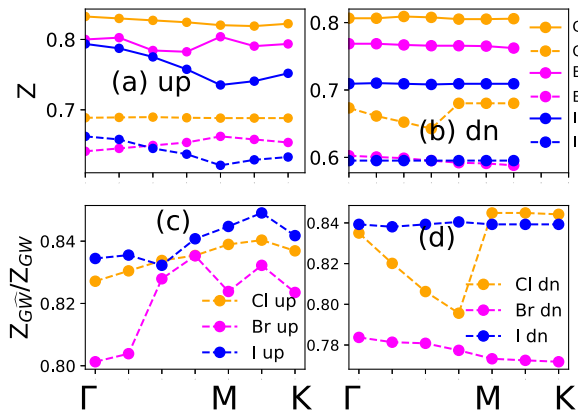


FIG. 8. CrX_3 : Real part of $\Sigma(k, \omega)$ is analyzed to extract the quasiparticle renormalization factor Z_k from the quasiparticle self-consistent GW (QSGW) and its self-consistent extension (QSGW \hat{W}). (a) and (b) The weak momentum dependence of the Z_k for the topmost valence band at the quasiparticle peaks at the k points chosen along the high-symmetry directions of the first Brillouin zone for the up and down spin sectors, respectively. (c) and (d) The relative suppression of the Z_k factor in QSGW \hat{W} compared with QSGW for the up and down spin sectors, respectively.

and the orbital character of the valence band. Many-body effects both enhance the band gap and make the valence band eigenfunctions more directional. We also showed that addition of ladder diagrams to improve W increases the screening, thus softening the many-body corrections to LDA. Further, we quantify the momentum dependence of the self-energies at different levels of the theory and show explicitly how excitonic correlations lead to renormalization of the electronic bands and localization of charges. As the hybridization between $\text{Cr } d$ and $X p$ enhances in the direction $\text{Cl} \rightarrow \text{Br} \rightarrow \text{I}$, the systems become more bandlike with lesser electronic correlations. In the same sequence as the $X p$ states become shallower with respect to the $\text{Cr } d$ states, we show explicitly that weak perturbations can significantly modify the hybridization, thereby leading to qualitative changes in the valence band features. Summarily, we show how a starting point independent implementation of GW and BSE leads to changes in electronic band energies and wave functions via complicated interplay between charge and self-energy self-consistencies in CrX_3 .

ACKNOWLEDGMENTS

M.I.K., A.N.R., and S.A. are supported by the ERC Synergy Grant, Project No. 854843 FASTCORR (ultrafast dynamics of correlated electrons in solids). M.v.S. and D.P. are

TABLE III. Shown are the $\text{Cr } d$ occupancies.

Variants	CrCl_3	CrBr_3	CrI_3
LDA	4.23	4.44	4.66
QSGW	4.08	4.3	4.66
BSE	4.11	4.35	4.64

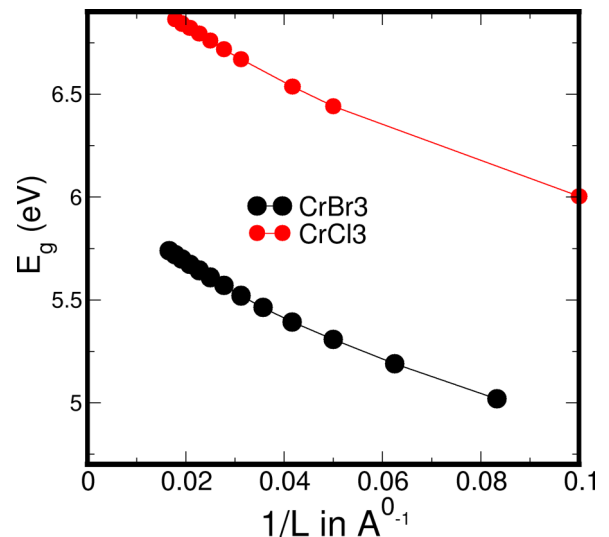


FIG. 9. CrBr_3 and CrCl_3 : Scaling of the one particle band gap from QSGW with vacuum size L .

supported by the Simons Many-Electron Collaboration. We acknowledge PRACE for awarding us access to Irene-Rome hosted by TGCC, France, and Jewels Booster and Clusters, Germany; STFC Scientific Computing Department's SCARF cluster, Cambridge Tier-2 system operated by the University of Cambridge Research Computing Service [43] funded by EPSRC Tier-2 capital Grant No. EP/P020259/1. M.v.S. was supported by DOE grant KC0310010-ERW7246.

APPENDIX A: NUMERICAL DETAILS

Single-particle calculations [LDA, and energy band calculations with the static quasiparticlized QSGW self-energy $\Sigma^0(k)$] were performed on a $16 \times 16 \times 1$ k -mesh, while the (relatively smooth) dynamical self-energy $\Sigma(k)$ was constructed using a $6 \times 6 \times 1$ k -mesh and $\Sigma^0(k)$ extracted from it. For each iteration in the QSGW self-consistency cycle, the charge density was made self-consistent. The QSGW cycle was iterated until the root mean square (RMS) change in Σ^0 reached 10^{-5} Ry. Thus, the calculation was self-consistent in both $\Sigma^0(k)$ and the density. Numerous checks were made to verify that the self-consistent $\Sigma^0(k)$ was independent of starting point, for both QSGW and QSGW \hat{W} calculations, e.g., using

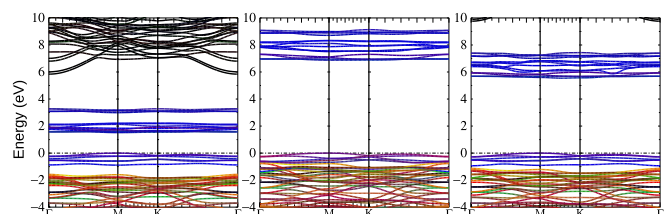


FIG. 10. CrCl_3 : The colors correspond to $\text{Cl } p_x + p_y$ (red), $\text{Cl } p_z$ (green), and $\text{Cr } d$ (blue) [from left to right: local density approximation (LDA), quasiparticle self-consistent GW (QSGW), and its self-consistent extension (QSGW \hat{W}), respectively].

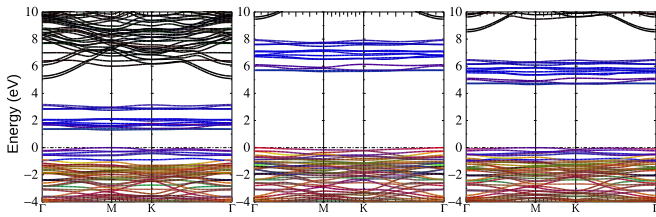


FIG. 11. CrBr_3 : The colors correspond to Br $p_x + p_y$ (red), Br p_z (green), and Cr d (blue) [from left to right: local density approximation (LDA), quasiparticle self-consistent GW (QSGW), and its self-consistent extension ($QSG\hat{W}$), respectively).

LDA or Hartree-Fock self-energy as the initial self-energy for QSGW and using LDA or QSGW as the initial self-energy for $QSG\hat{W}$.

For this paper, the electron-hole two-particle correlations are incorporated within a self-consistent ladder BSE implementation [31,32] with Tamm-Dancoff approximation [44,45]. The effective interaction W is calculated with ladder BSE corrections and the self-energy, using a static vertex in the BSE. Here, G and W are updated iteratively until all of them converge, and this is what we call $QSG\hat{W}$. Ladders increase the screening of W , reducing the gap in addition to softening the LDA \rightarrow QSGW corrections noted for the valence bands.

For all materials, we checked the convergence in the $QSG\hat{W}$ band gap by increasing the size of the two-particle Hamiltonian. We increased the number of valence and conduction states that were included in the two-particle Hamiltonian. We observed that, for all materials, the $QSG\hat{W}$ band gap stopped changing once 24 valence and 24 conduction states were included in the two-particle Hamiltonian. While the gap was most sensitive to the number of valence states, 14 conducting states produced results within 2% error of the converged results from 24 conduction states.

In Table III, we list the Cr d occupancies for different materials at different levels of the theory.

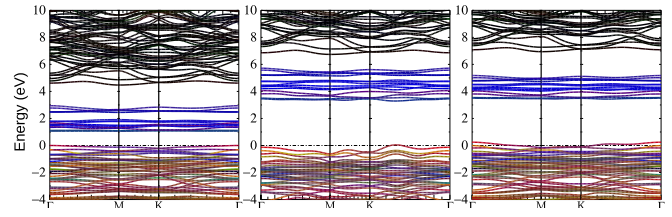


FIG. 12. CrI_3 : The colors correspond to I $p_x + p_y$ (red), I p_z (green), and Cr d (blue) [from left to right: local density approximation (LDA), quasiparticle self-consistent GW (QSGW), and its self-consistent extension ($QSG\hat{W}$), respectively).

APPENDIX B: VACUUM DISTANCE SCALING

Periodic boundary conditions were used in all directions, introducing an unwanted coupling between CrBr_3 slabs. To minimize this coupling, a vacuum of length L was inserted between slabs, and L was varied.

The QSGW is known to fix the infamous gap problem [46] in insulators. We observed that the band gap increased significantly in all three compounds within QSGW: 6.87 eV in Cl, 5.73 eV in Br, and 3.25 eV in I (see Table I). We changed the vacuum length from 10 to 80 Å and observed the scaling of the band gap with vacuum size (L). We observed an almost perfect $1/L$ scaling (see Fig. 9) of the gap, as noted earlier in a separate work on V_2O_5 [47]. This also allowed us to check the dielectric constant (ϵ_∞) and its vacuum correction. In the limit of a purely freestanding ML, all three directional components of the macroscopic dielectric response in the static limit approached 1, suggesting the absence of screening. We used this vacuum length (60 Å) for the rest of the discussions in this paper.

APPENDIX C: FULL BAND STRUCTURES

In Figs. 10–12, we show the band structures for all materials over larger energy windows.

- [1] B. Huang, G. Clark, E. Navarro-Moratalla, D. R. Klein, R. Cheng, K. L. Seyler, D. Zhong, E. Schmidgall, M. A. McGuire, D. H. Cobden *et al.*, *Nature (London)* **546**, 270 (2017).
- [2] D. R. Klein, D. MacNeill, J. L. Lado, D. Soriano, E. Navarro-Moratalla, K. Watanabe, T. Taniguchi, S. Manni, P. Canfield, J. Fernández-Rossier *et al.*, *Science* **360**, 1218 (2018).
- [3] Z. Zhang, J. Shang, C. Jiang, A. Rasmata, W. Gao, and T. Yu, *Nano Lett.* **19**, 3138 (2019).
- [4] M. Kim, P. Kumaravadeivel, J. Birkbeck, W. Kuang, S. G. Xu, D. Hopkinson, J. Knolle, P. A. McClarty, A. Berdyugin, M. B. Shalom *et al.*, *Nat. Electron.* **2**, 457 (2019).
- [5] X. Cai, T. Song, N. P. Wilson, G. Clark, M. He, X. Zhang, T. Taniguchi, K. Watanabe, W. Yao, D. Xiao *et al.*, *Nano Lett.* **19**, 3993 (2019).
- [6] C. Gong, L. Li, Z. Li, H. Ji, A. Stern, Y. Xia, T. Cao, W. Bao, C. Wang, Y. Wang *et al.*, *Nature (London)* **546**, 265 (2017).
- [7] Z. Fei, B. Huang, P. Malinowski, W. Wang, T. Song, J. Sanchez, W. Yao, D. Xiao, X. Zhu, A. F. May *et al.*, *Nat. Mater.* **17**, 778 (2018).
- [8] Y. Deng, Y. Yu, M. Z. Shi, Z. Guo, Z. Xu, J. Wang, X. H. Chen, and Y. Zhang, *Science* **367**, 895 (2020).
- [9] C. Gong and X. Zhang, *Science* **363**, eaav4450 (2019).
- [10] M. Gibertini, M. Koperski, A. Morpurgo, and K. Novoselov, *Nat. Nanotechnol.* **14**, 408 (2019).
- [11] N. D. Mermin and H. Wagner, *Phys. Rev. Lett.* **17**, 1133 (1966).
- [12] V. Y. Irkhin, A. A. Katanin, and M. I. Katsnelson, *Phys. Rev. B* **60**, 1082 (1999).
- [13] D. Soriano, M. I. Katsnelson, and J. Fernández-Rossier, *Nano Lett.* **20**, 6225 (2020).
- [14] S. Jiang, L. Li, Z. Wang, K. F. Mak, and J. Shan, *Nat. Nanotechnol.* **13**, 549 (2018).
- [15] S. Jiang, J. Shan, and K. F. Mak, *Nat. Mater.* **17**, 406 (2018).

- [16] Z. Wang, T. Zhang, M. Ding, B. Dong, Y. Li, M. Chen, X. Li, J. Huang, H. Wang, X. Zhao *et al.*, *Nat. Nanotechnol.* **13**, 554 (2018).
- [17] M. Bonilla, S. Kolekar, Y. Ma, H. C. Diaz, V. Kalappattil, R. Das, T. Eggers, H. R. Gutierrez, M.-H. Phan, and M. Batzill, *Nat. Nanotechnol.* **13**, 289 (2018).
- [18] S. Jiang, L. Li, Z. Wang, J. Shan, and K. F. Mak, *Nature Electronics* **2**, 159 (2019).
- [19] T. Song, X. Cai, M. W.-Y. Tu, X. Zhang, B. Huang, N. P. Wilson, K. L. Seyler, L. Zhu, T. Taniguchi, K. Watanabe *et al.*, *Science* **360**, 1214 (2018).
- [20] T. Song, M. W.-Y. Tu, C. Carnahan, X. Cai, T. Taniguchi, K. Watanabe, M. A. McGuire, D. H. Cobden, D. Xiao, W. Yao *et al.*, *Nano Lett.* **19**, 915 (2019).
- [21] Z. Wang, I. Gutiérrez-Lezama, N. Ubrig, M. Kroner, M. Gibertini, T. Taniguchi, K. Watanabe, A. Imamoğlu, E. Giannini, and A. F. Morpurgo, *Nat. Commun.* **9**, 2516 (2018).
- [22] H. H. Kim, B. Yang, T. Patel, F. Sfigakis, C. Li, S. Tian, H. Lei, and A. W. Tsen, *Nano Lett.* **18**, 4885 (2018).
- [23] I. Kashin, V. Mazurenko, M. Katsnelson, and A. Rudenko, *2D Mater.* **7**, 025036 (2020).
- [24] Y. O. Kvashnin, A. Bergman, A. I. Lichtenstein, and M. I. Katsnelson, *Phys. Rev. B* **102**, 115162 (2020).
- [25] D. Soriano, A. N. Rudenko, M. I. Katsnelson, and M. Rösner, [arXiv:2103.04686](https://arxiv.org/abs/2103.04686) [cond-mat.str-el].
- [26] A. Molina-Sanchez, G. Catarina, D. Sangalli, and J. Fernandez-Rossier, *J. Mater. Chem. C* **8**, 8856 (2020).
- [27] S. V. Streltsov and D. I. Khomskii, *Phys. Usp.* **60**, 1121 (2017).
- [28] D. Soriano, C. Cardoso, and J. Fernández-Rossier, *Solid State Commun.* **299**, 113662 (2019).
- [29] M. van Schilfgaarde, T. Kotani, and S. Faleev, *Phys. Rev. Lett.* **96**, 226402 (2006).
- [30] D. Pashov, S. Acharya, W. R. Lambrecht, J. Jackson, K. D. Belashchenko, A. Chantis, F. Jamet, and M. van Schilfgaarde, *Comput. Phys. Commun.* **249**, 107065 (2020).
- [31] B. Cunningham, M. Grüning, P. Azarhoosh, D. Pashov, and M. van Schilfgaarde, *Phys. Rev. Mater.* **2**, 034603 (2018).
- [32] B. Cunningham, M. Grüning, D. Pashov, and M. van Schilfgaarde, [arXiv:2106.05759](https://arxiv.org/abs/2106.05759) [cond-mat.mtrl-sci].
- [33] S. Albrecht, L. Reining, R. Del Sole, and G. Onida, *Phys. Rev. Lett.* **80**, 4510 (1998).
- [34] M. Rohlfing and S. G. Louie, *Phys. Rev. B* **62**, 4927 (2000).
- [35] A. N. Chantis, M. van Schilfgaarde, and T. Kotani, *Phys. Rev. Lett.* **96**, 086405 (2006).
- [36] C. Bhandari, M. van Schilfgaarde, T. Kotani, and W. R. L. Lambrecht, *Phys. Rev. Mater.* **2**, 013807 (2018).
- [37] D. Deguchi, K. Sato, H. Kino, and T. Kotani, *Jpn. J. Appl. Phys.* **55**, 051201 (2016).
- [38] M. Wu, Z. Li, T. Cao, and S. G. Louie, *Nat. Commun.* **10**, 2371 (2019).
- [39] A. Kundu, Y. Liu, C. Petrovic, and T. Valla, *Sci. Rep.* **10**, 15602 (2020).
- [40] Y. Lee, T. Kotani, and L. Ke, *Phys. Rev. B* **101**, 241409(R) (2020).
- [41] A. L. Kutepov, *Phys. Rev. Materials* **5**, 083805 (2021).
- [42] M. Wu, Z. Li, and S. G. Louie, [arXiv:2106.00770](https://arxiv.org/abs/2106.00770) [cond-mat.mtrl-sci].
- [43] <https://www.hpc.cam.ac.uk>
- [44] S. Hirata and M. Head-Gordon, *Chem. Phys. Lett.* **314**, 291 (1999).
- [45] G. Myrta, A. Marini, and X. Gonze, *Nano Lett.* **9**, 2820 (2009).
- [46] F. Aryasetiawan and O. Gunnarsson, *Rep. Prog. Phys.* **61**, 237 (1998).
- [47] C. Bhandari, W. R. L. Lambrecht, and M. van Schilfgaarde, *Phys. Rev. B* **91**, 125116 (2015).